JVI Journals.ASM.org

Structure, Adsorption to Host, and Infection Mechanism of Virulent Lactococcal Phage p2

Cecilia Bebeacua,[a,b,c]* Denise Tremblay,[d] Carine Farenc,[a,b] Marie-Pierre Chapot-Chartier,[f] Irina Sadovskaya,[g] Marin van Heel,[c]* David Veesler,[a,b]* Sylvain Moineau,[d,e] Christian Cambillau[a,b]

Aix-Marseille Université, Architecture et Fonction des Macromolécules Biologiques, UMR 7257, Marseille, France[a]; Centre National de la Recherche Scientifique, Architecture et Fonction des Macromolécules Biologiques, UMR 7257, Marseille, France[b]; Department of Biological Sciences, Imperial College London, London, United Kingdom[c]; Groupe de Recherche en Écologie Buccale (GREB) and Félix d'Hérelle Reference Center for Bacterial Viruses, Faculté de Médecine Dentaire, Université Laval, Québec City, Québec, Canada[d]; Département de Biochimie, Microbiologie et Bio-Informatique, Faculté des Sciences et de Génie, Université Laval, Québec City, Québec, Canada[e]; INRA and AgroParisTech, UMR1319 Micalis, Jouy-en-Josas, France[f]; Université Lille Nord de France, Lille, France, and Université du Littoral-Côte d'Opale, LR2B/UMT 08, Bassin Napoléon, Boulogne-sur-Mer, France[g]

Lactococcal siphophages from the 936 and P335 groups infect the Gram-positive bacterium *Lactococcus lactis* using receptor binding proteins (RBPs) attached to their baseplate, a large multiprotein complex at the distal part of the tail. We have previously reported the crystal and electron microscopy (EM) structures of the baseplates of phages p2 (936 group) and TP901-1 (P335 group) as well as the full EM structure of the TP901-1 virion. Here, we report the complete EM structure of siphophage p2, including its capsid, connector complex, tail, and baseplate. Furthermore, we show that the p2 tail is characterized by the presence of protruding decorations, which are related to adhesins and are likely contributed by the major tail protein C-terminal domains. This feature is reminiscent of the tail of *Escherichia coli* phage λ and *Bacillus subtilis* phage SPP1 and might point to a common mechanism for establishing initial interactions with their bacterial hosts. Comparative analyses showed that the architecture of the phage p2 baseplate differs largely from that of lactococcal phage TP901-1. We quantified the interaction of its RBP with the saccharidic receptor and determined that specificity is due to lower k_{off} values of the RBP/saccharidic dissociation. Taken together, these results suggest that the infection of *L. lactis* strains by phage p2 is a multistep process that involves reversible attachment, followed by baseplate activation, specific attachment of the RBPs to the saccharidic receptor, and DNA ejection.

Bacteriophages, viruses of bacteria, are found in various numbers in most, if not all, ecosystems. Their ability to persist in these diverse environments stems from their effectiveness in recognizing and replicating in their bacterial hosts. Moreover, their remarkable genome plasticity and diversity allow them to evolve when facing various selective forces. However, phages can be classified into a relatively small number of families. Tailed phages with double-stranded genomes are by far the most studied bacterial viruses, as over 95% of the known phages are grouped within the *Caudovirales* order (1). The latter is divided into three families (*Myoviridae*, *Siphoviridae*, and *Podoviridae*) based on the morphology of their tail, which contains the host recognition device at the distal end or through connected fibers. Each of these families is also divided into genera, species, and numerous groups.

Phages infecting *Lactococcus lactis* strains predominantly belong to the *Siphoviridae* family, which is characterized by a long, flexible, noncontractile tail. They also represent one of the most documented phage groups in the viral databases (2). The interest in these phages is fueled by the mostly negative impact that the virulent members have on milk fermentation, as they infect and lyse the drivers of this industrial process, namely, *L. lactis* starter cultures (3). To date, lactococcal phages isolated worldwide have been classified into 10 genetically distinct groups (2); however, only 3 of them are predominant and contain numerous members, namely, the 936, c2, and P335 groups. While virulent c2-like phages have been shown to start their lytic infection cycle through the recognition of a host integral membrane protein called Pip (4, 5), members of the 936 and P335 groups are believed to recognize, in a strain-specific way, phosphopolysaccharides forming an external cell wall layer of *L. lactis*, the pellicle (6).

Recent structure-function analyses of lactococcal phages indicated that these viruses represent useful models for the study of saccharide-recognizing *Siphoviridae*. The structures of several receptor binding proteins (RBPs) have been determined, including those of 936-like phages p2 and bIL170 as well as the P335-like phage TP901-1 (7–11). The primary role of RBPs, which are located at the tip of the tail, is to allow the phage to recognize its specific receptor at the cell surface. Chimeric RBPs were also constructed to demonstrate that their C-terminal domain, also called the head domain, was particularly involved in this precise host recognition process (12). Next, the crystal structures of the protein complex connecting the RBP to the rest of the phage tail, the baseplate, were also solved for siphophages p2 and TP901-1 (13–15). The electron microscopy (EM) reconstruction of the whole phage TP901-1 was recently reported, as was a composite EM model of this gigantic molecular machine (16). Finally, each of the trimeric RBPs has been demonstrated to harbor three saccharide

Received 21 July 2013 **Accepted** 30 August 2013

Published ahead of print 11 September 2013

Address correspondence to Sylvain Moineau, sylvain.moineau@bcm.ulaval.ca, or Christian Cambillau, cambillau@afmb.univ-mrs.fr.

* Present address: Cecilia Bebeacua, Structural and Computational Biology & Cell Biology and Biophysics, EMBL, Heidelberg, Germany; Marin van Heel, NeCEN, Leiden, The Netherlands; David Veesler, Structural Virology, Department of Integrative Structural and Computational Biology, Scripps Research Institute, La Jolla, California, USA.

doi:10.1128/JVI.02033-13

TABLE 1 Summary of data of lactococcal phage p2 single-particle EM reconstructions

Structure	Method	Symmetry	Resolution (Å)	No. of particles
Capsid	Cryo-EM	Icosahedral	13	3,329
Connector	Negative staining	C12	21	1,500
Tail	Negative staining	Helicoidal	22	2,171
Baseplate	Negative staining	C6	22	10,000

binding sites, which can be neutralized along with the infection process by a camelid nanobody (9, 10, 17–19). Among others, it was proposed that the phage adsorption architectures have evolved in correlation with the nature of the receptors found on the host cell surface.

Interestingly, in the case of phage p2 (936), both the crystal structure of the baseplate and the electron microscopy map of the free virions showed that this phage contains 18 RBPs. Furthermore, in the baseplate, these host recognition (head) domains pointed upwards, toward the capsid rather than toward the host. However, the presence Ca^{2+} ions in crystallization studies led to a significant conformational change of the baseplate, leading to a 200° downward rotation of the RBPs, thereby presenting their binding sites to the host (14). Concurrently, a channel opens up at the bottom, which is wide enough for DNA passage. On the other hand, phage TP901-1 (P335 subgroup II [20]) exhibits a ready-to-infect baseplate, as its 54 RBP recognition domains are already oriented toward the host receptors (15). Noteworthy is that the members of the 936 group require Ca^{2+} ions for infection, while those of P335 subgroup II (20) do not (15).

A number of EM reconstructions have been reported for complete *Podoviridae* phages (21–23), as they are more prone to single-particle analysis due to their rigidity. The structures of some *Siphoviridae* phages are also available, such as those of *Escherichia coli* phage T5 (24), *Bacillus subtilis* phage SPP1 (25–27), phage TP901-1 (16), and mycobacteriophage Araucaria (28). Due to the inherent flexibility of siphophages, their EM structure determinations have relied on a "divide-and-conquer" approach, where the different parts of the virion are reconstructed independently and then combined to yield the structure of the whole phage (16, 28).

Here, we report the full virion structure of the strictly lytic phage p2, the archetype member of the lactococcal 936 group, obtained by using single-particle electron microscopy. One of the most interesting features observed in the virion is the presence of a decorated tail. We characterized the binding of the p2 and TP901-1 RBPs to the pellicle saccharide and found that k_{off} is the most important feature for interaction. These observations lead us to propose the hypothesis of a three-step mechanism of adhesion of the p2 virion to its host.

MATERIALS AND METHODS

Phage production and purification. *L. lactis* MG1363, the host of phage p2, was grown in GM17 (M17 supplemented with 0.5% glucose). For phage amplification, $CaCl_2$ was added to the medium at a final concentration of 10 mM. Phage p2 was amplified and purified as reported previously (29). Purified phages were conserved at 4°C in buffer (50 mM Tris-HCl [pH 7.5], 100 mM NaCl, 8 mM $MgSO_4$) (30).

Specimen preparation. Negative staining and cryo-EM grids were prepared as previously described (14). Briefly, 3 μl of CsCl-purified phage sample was applied onto glow-discharged carbon-coated grids (Holey Quantifoil grids for cryo-EM) and either stained with 2% uranyl acetate solution (negative staining) or plunged into liquid ethane for vitrification by using an FEI Vitrobot instrument (cryo-EM, capsid).

Data collection and image processing. One thousand negatively stained images and 150 charge-coupled-device (CCD) cryo-EM images were collected by using a Phillips CM200 microscope at magnifications of ×38,000 and ×50,000, respectively. All processing was carried out by using IMAGIC software (31). Defocus estimation and correction for the microscope contrast transfer function (CTF) were carried out by using the IMAGIC CTF2D_FIND and CTF2D_FLIP programs. Particles were selected by using the program PICK_M_ALL (Table 1) and extracted into boxes of 200 by 200 pixels, 128 by 128 pixels, and 50 by 50 pixels, for the capsid, the connector, and the tail, respectively. These sets of particles were further combined into three different data sets. In addition, to evaluate the overall dimension of the tail and the number of tail rings, 1,000 isolated phage particles with a straight tail were manually selected from the negative staining images, extracted into boxes of 300 by 300 pixels (coarsened by 4), and combined into a data set. Data sets were pretreated and submitted to alignment by classification. Tail fragments were properly aligned as they were boxed, including a fragment of either the baseplate or the connector. Initial models were built to form a visually selected class average representing a side view imposing the corresponding symmetry: C6 for the full phage and tail, C12 for the connector, and icosahedral for the capsid (Table 1). The initial models were then refined by projection matching with a sampling rate of 5°. As previously described (14), particles were always in a sideways orientation, with the symmetry axis perpendicular to the projection direction. Therefore, maps were reprojected along the equator (IMAGIC Euler angle β, equal to 90°), with a difference of 20°. After refinements, final models were obtained at resolutions of approximately 13 Å for the capsid, 21 Å for the connector, and 22 Å for the tail, as estimated by Fourier shell correlation (FSC) and the 1/2-bit threshold criterion (32) (Table 1 and Fig. 1).

Tail helical processing. The tail particles, aligned as described above, were submitted to helical processing. The helical map was produced by using the package IHRSR++ (33). The rotational symmetry used was C6, and, as the particles were already aligned, the maximum allowed in-plane rotational angle was set to 10°. The initial helical parameters were determined by using the Brandeis Helical Package (34) to calculate the Bessel orders of the basic layer lines (6 and −6). These were later refined by IHRSR++ to a helical rise of 37.4 Å and a rotation between subunits of 46.3°.

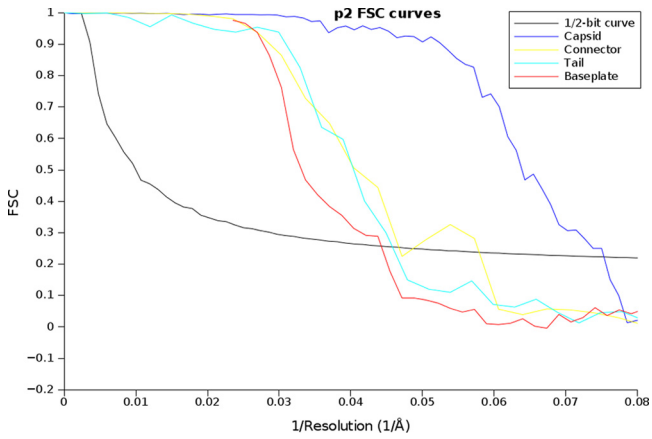

FIG 1 Fourier shell correlation (FSC) curves of the final three-dimensional reconstructions. These curves were obtained by correlation of two different three-dimensional images created by splitting the particle set into two subsets. The resolutions were estimated by FSC and the 1/2-bit cutoff threshold criterion as 13 Å for the capsid, 21 Å for the connector, 21 Å for the helical tail, and 25 Å for the baseplate.

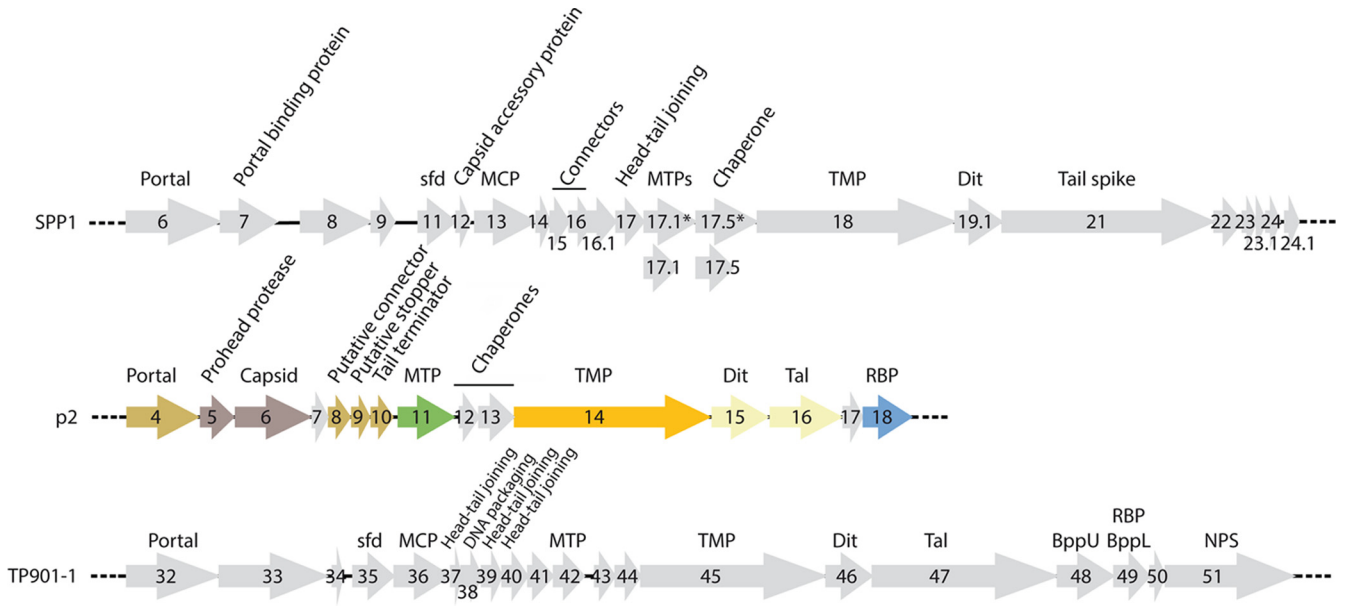

FIG 2 Schematic representation and assignment of the structural gene modules of phages p2, SPP1, and TP901-1. Genes coding for nonstructural ORFs are in light gray. The colors correspond to the colors in Fig. 2 and 4 to 6. The capsid and portal complex ORFs are in dark gray and dark yellow, respectively. The genes coding for the tail and baseplate ORFs are in green, orange, light yellow, and blue. Sfd, scaffolding; MCP, major capsid protein, MTP, major tail protein, TMP, tail tape measure protein; Dit, distal tail protein; Tal, tail-associated lysine; RBP, receptor binding protein; BppU, baseplate upper protein; BppL, baseplate lower protein; NPS, neck passage structure.

Fitting and structure visualization. Molecular graphics and analyses were performed with the UCSF Chimera package, available at the Resource for Biocomputing, Visualization, and Informatics of the University of California—San Francisco (supported by NIGMS grant P41-GM103311). The model/EM map or EM map/EM map fitting was performed by the option "fit in map" of the "volume" register. The difference maps were calculated by the "vop substract" command.

Surface plasmon resonance. The surface plasmon resonance (SPR) binding experiments were performed with a BIAcore T-200 instrument (GE Healthcare). The matrix-free surface C1 sensor chip, HBS-P buffer (10 mM HEPES [pH 7.4], 150 mM NaCl, 0.005% [vol/vol] surfactant P20), and the amine coupling kit were purchased from GE Healthcare. The sensor chip was first conditioned according to the manufacturer's recommendations and then equilibrated in running buffer. The pellicle extract from *L. lactis* MG1363 was obtained as described previously (6). The coupling reaction was performed as described previously (35). The RBP head domain (host recognition) of phage p2 and the trimeric RBP of phage TP901-1 were expressed and purified as described previously (8, 10). All SPR experiments were performed at 25°C, with a flow rate of 10 μl/min. The activation of the surface was performed with a 1:1 mixture of 0.1 M *N*-ethyl-*N*′-(dimetheylamino-propyl)carbodiimide (EDC) and 0.1 M *N*-hydroxysuccinimide (NHS). Streptavidin (Sigma-Aldrich) was injected over the surface in 10 mM sodium acetate buffer (pH 5.5), and ~3,000 response units (RU) of streptavidin was immobilized. The remaining *N*-hydroxysuccinimide esters were deactivated with a pulse of 1 M ethanolamine (pH 8.5). The dried biotinylated pellicle extract was diluted in water and injected over the target surface (Fc2), resulting in immobilization at a level of 160 RU. Biotin (Sigma-Aldrich) was injected onto the reference surface (Fc1) and reached immobilization at a level of 20 RU. The RBP head domain of phage p2 and the trimeric RBP of phage TP901-1 were diluted to five decreasing concentrations in running buffer and analyzed by passing them on the immobilized pellicle extract. The ligand surface was regenerated with 10 mM HCl. The sensorgrams were processed by using the double-referencing method (36). First, the binding response from the reference surface was subtracted from the binding response of the surface containing the immobilized pellicle extract to correct for bulk refractive index changes. Second, the response from an average of the blank injections was subtracted to remove any systematic artifacts observed between the reaction and the reference flow cell. The K_d (equilibrium dissociation constant) values were obtained by using GraphPad Prism version 5.0 for Macintosh (GraphPad Software, La Jolla, CA, USA).

Protein structure accession numbers. The capsid, connector, and tail reconstructions have been deposited at the EMDB with accession numbers EMD-2462, EMD-2463, and EMD-2464, respectively.

RESULTS

Sequence analysis of the structural cassette. Bioinformatics and proteome analyses of the p2 virion indicated that it contains 12 distinct structural proteins (Fig. 2 and Table 2), namely, open reading frames (ORFs) 4 to 11, 14 to 16, and 18. The nonstructural ORF-12 was previously proposed to be a putative chaperone (37), and this might also be the case for ORF-13, while the nonstructural ORF-17 has an unknown function. The structural gene cassette is therefore very compact compared to the ones of lactococcal phage TP901-1 (38) and *B. subtilis* phage SPP1 (39). The annotation of the phage p2 structural cassette was revealed to be challenging due to the limited number of hits obtained by using sequence analysis software. Because the baseplate crystal structure has been determined already, it was possible to assign ORFs 15, 16, and 18 to Dit (distal tail protein), Tal (tail-associated lysin), and RBP, respectively (14) (Fig. 2 and Table 2). BLAST analysis of the other structural proteins yielded significant hits for ORF-4 (portal), ORF-5 (capsid maturation protease), and ORF-14 (tape measure protein [TMP]). HHpred indicated that ORF-6 was the major capsid protein (MCP), whereas the ORF-11 C-terminal domain appeared to be related to adhesins. In fact, the attributions of MCP to ORF-6 and major tail protein (MTP) to ORF-11 were recently confirmed by using immunoelectron microscopy of

TABLE 2 Phage p2 ORF assignments[a]

ORF	Start position	Stop position	Size (aa)	Molecular mass (kDa)	pI	Putative function	Abbreviation	Protein description	Assignment
1	274	798	174	19.9	5.2	Terminase small subunit		NS	seq. Id.
2	799	2421	540	62.9	5.8	Terminase large subunit		NS	seq. Id.
3	2411	2695	94	11.1	8.9	Endonuclease		NS	seq. Id.
4	2708	3844	378	43.2	5.1	Portal protein	Portal	Structural	HHpred
5	3825	4361	178	12.3	4.5	Prohead protease		Structural	HHpred
6	4354	5535	393	44.3	5.5	Major capsid protein	MCP	Structural	Immuno
7	5556	5819	87	10.0	6.2	Chaperone gpFI		NS	seq. Id.
8	5819	6133	104	11.9	8.9	Connector?	HCP1	Structural	Position/size
9	6123	6461	112	12.7	4.1	Stopper?	HCP2	Structural	Position/size
10	6452	6817	121	13.7	10.0	Tail terminator	TT	Structural	Position/size
11	6830	7735	301	32.4	4.9	Major tail protein	MTP	Structural	Immuno
12	7786	8061	91	10.6	4.9	Chaperone		NS	X ray
13	8081	8593	170	19.9	4.9	Chaperone		NS	Position
14	8593	11592	999	104.4	8.7	Tape measure protein	TMP	Structural	Position/size
15	11592	12488	298	34.5	5.4	Tail distal	Dit	Structural	X ray
16	12488	13615	375	42.8	5.3	Tail lysozyme-like	Tal	Structural	X ray
17	13605	13898	97	11.4	9.4	Putative protein		NS	
18	13888	14682	264	28.6	6.8	Receptor binding protein	RBP	Structural	X ray

[a] aa, amino acids; NS, nonstructural.

phage p2 and antibodies specific for the two ORFs (40). ORF-7 was putatively assigned as a gpFI-like chaperone due to the location of its gene (and its size) in the genome of p2 and comparison with the genome of lambda (40). The gene coding for the tail terminator (TT), being generally located upstream of the gene coding for MTP, could therefore be assigned to *orf-10*, whose protein product has a predicted number of amino acid residues close to that of the TT of TP901-1 (121 residues and 129 residues, respectively). Finally, ORF-8 and ORF-9 are likely two capsid completion proteins (Table 2), as they exhibit lengths comparable to those of the equivalent TP901-1 proteins (Fig. 2 and Table 3).

Electron microcopy reconstruction of the full phage structure. The tail flexibility of siphophages prevented electron microscopy studies of p2 virions as a whole, which is in contrast with the compact podophages (22). We thus reconstructed the p2 virion as four separate regions using the appropriate local symmetry (capsid, connector complex, tail, and baseplate) (Table 1) before recapitulating *in silico* the whole phage using a low-resolution reconstruction obtained from a few straight phages, as described previously (16, 28) (Fig. 3). The p2 virion is ~2,100 Å long and is assembled from an icosahedral capsid plugged via a connector to the relatively long noncontractile tail, whose extremity is decorated by a baseplate.

The capsid. Phage capsids carry and protect the viral genome, which is packaged within their interior (41). These protein capsids are solid devices, since DNA exerts a very high pressure on their walls (42). We obtained a cryo-EM reconstruction of the p2 capsid at a 13-Å resolution using 3,329 particle images and applying icosahedral symmetry (Table 1 and Fig. 4A). The DNA-filled mature capsid is ~690 Å wide along its 5-fold axes and harbors 60 hexamers and 11 pentamers of the ORF-6 MCP, organized with a T=7 symmetry (Fig. 3 and 4). A dodecamer of the portal protein occupies the 12th vertex position, and its density has been averaged out in the capsid reconstruction process, due to the application of icosahedral symmetry. We thus independently investigated the connector structure by carrying out a reconstruction of this region only. The capsid cavity is filled with the double-stranded DNA (dsDNA) genome (27,595 bp), arranged as concentric layers regularly spaced by ~25 Å (Fig. 4B), a feature observed in other members of the *Caudovirales* order (41). All reported tailed-phage MCP structures feature the so-called *E. coli* siphophage HK97 or Johnson fold that is also shared by herpesviruses and some archaeal viruses (41, 43, 44). We expected the lactococcal p2 MCP to exhibit a similar fold, as suggested by the results of the analysis of the ORF-6 amino acid sequence by the HHpred server. We therefore built a pseudoatomic model of the p2 capsid by rigid-body fitting of the icosahedral asymmetric unit coordinates of the mature HK97 capsid (PDB accession number 1OHG) within the EM reconstruction (Fig. 4A). It is noteworthy that the p2 MCP has been found to be cross-linked by proteomics analyses (40). The seven subunits of the icosahedral asymmetric unit are well accommodated in the p2 capsid EM density and form an ~30-Å-thick protein layer around the DNA. The pentons protrude significantly above the capsid surface by ~40 Å, a feature observed in other phages (such as TP901-1) but to a lesser extent (Fig. 4, inset).

The head-to-tail connecting region. The connector is a protein complex located at a unique capsid vertex where it replaces a penton motif (Fig. 5A to C). It links the capsid to the phage tail and forms a channel involved in packaging of the phage genomic DNA inside the capsid during phage assembly within the infected bacterial cell. The connector is also involved in phage DNA release from the capsid and subsequent entry into the bacterial cells at the onset of infection and after the host recognition process by the phage RBPs. The connector is often assembled from three different components forming successive rings with 12-fold symmetry: the portal and the first head completion protein, both exhibiting an open central channel, and the stopper, which closes the channel to prevent phage DNA leakage from the capsid after packaging inside the infected bacterial cell. The stopper protein mediates the connection with the tail terminator protein. The phage p2 con-

TABLE 3 Comparison of p2 structural proteins with those of other characterized phages

Protein	ORF	No. of aa		
		p2	SPP1	TP901-1
Portal	4	378	503	452
MCP	6	393	324	272
Connector	8	104	102	110
Stopper	9	112	109	103
TT	10	121	134	129
MTP	11	301	177/266[a]	169
Dit	15	298	253	252
Tal	16	375	1,111	946

[a] Short/long forms.

nector was reconstructed at a 21-Å resolution by using ~1,500 particles and applying 12-fold symmetry along its channel axis (Table 1). The portal is a dodecamer unit with a conserved fold among tailed phages and herpesviruses (41, 43). The p2 portal protein (ORF-4) is smaller than the equivalent proteins of phages TP901-1 and SPP1 (378 versus 452 and 503 residues, respectively) (Table 3) but comparable to the coliphage HK97 portal protein (408 residues), with which it shares 24% sequence identity. Still, we used an SPP1 dodecameric portal model (45) to fit into the phage p2 connector reconstruction, as it yields the best correlation coefficient, indicative of the quality of the fit (Fig. 5D and E). We then docked the SPP1 gp15 dodecameric ring (PDB accession number 2KBZ) into the region of the connector reconstruction located directly beneath the portal (i.e., the first head completion protein), which is also well accommodated by the density.

The tail. We devised a strategy to obtain a topological template for the tail reconstruction and especially to obtain the number of tail MTP (ORF-11) rings in the p2 virion. We selected a few hundred phages with almost straight tails and used them for reconstruction of a low-resolution-scaffold 6-fold-averaged map (16, 28). In a following step, small tail segments were boxed and combined into one data set that was subsequently processed with the appropriate helical symmetry at a 22-Å resolution, using 2,171 particles (Table 1). These segments were then aligned on the low-resolution scaffold of the tail. This reconstruction made it possible to establish that the entire tail tube comprises 32 stacks, a tail terminator hexamer (ORF-10) located at the interface with the connector and 31 MTP (ORF-11) hexamers forming the tube, accounting for a total length of 1,160 Å (Fig. 6A).

The MTP hexamers exhibit domains protruding out of the tail tube and decorating it on its whole length. The external diameter of the tail tube is 165 Å, while its internal diameters are 115 Å and 85 Å at the interhexamer junction. Of note, the tail terminator has a diameter of ~110 Å and is devoid of decorations (Fig. 3). Each decoration of the tail tube forms a flat structure with dimensions of 20 by 30 Å. These motifs most likely result from the presence of a C-terminal domain in the p2 MTP that approximately doubles its number of amino acid residues relative to that of the phage TP901-1 MTP. However, the observed decorations appear too small to accommodate the whole MTP C-terminal domain, and we hypothesize that they probably oscillate around their anchoring positions, resulting in attenuation of their density. The 31 MTP hexameric rings are arranged with helical symmetry, characterized by a twist of 46.3° and a rise of 37.4 Å (Fig. 3 and 4).

The tail tube delineates an ~40-Å-wide central channel needed for the passage of the phage dsDNA from the capsid to its eventual entry into the cell (15, 25, 26, 45–47) (Fig. 6B and C). An elongated density is present inside the tail tube channel, and we attributed it to the tape measure protein ORF-14, the molecular ruler controlling tail length during phage assembly (48) (Fig. 6B and 5C).

The baseplate. A large macromolecular assembly, a host adsorption device or a baseplate, is often observed at the tail tip of *Siphoviridae* phages (13–16, 26, 28). We previously reported the crystal and EM structures (14) of the p2 baseplate, and we complete these results here by analyzing the baseplate in the context of the full virion. In a previous study (14), the p2 baseplate led to diffracting crystals (to 2.7 Å) only in the presence of RBP binding nanobodies (VHH5). However, the use of a nanobody led to the loss of a baseplate element, an ORF-15 (Dit) hexamer, compared to the cryo-EM structure of the purified baseplate without nano-

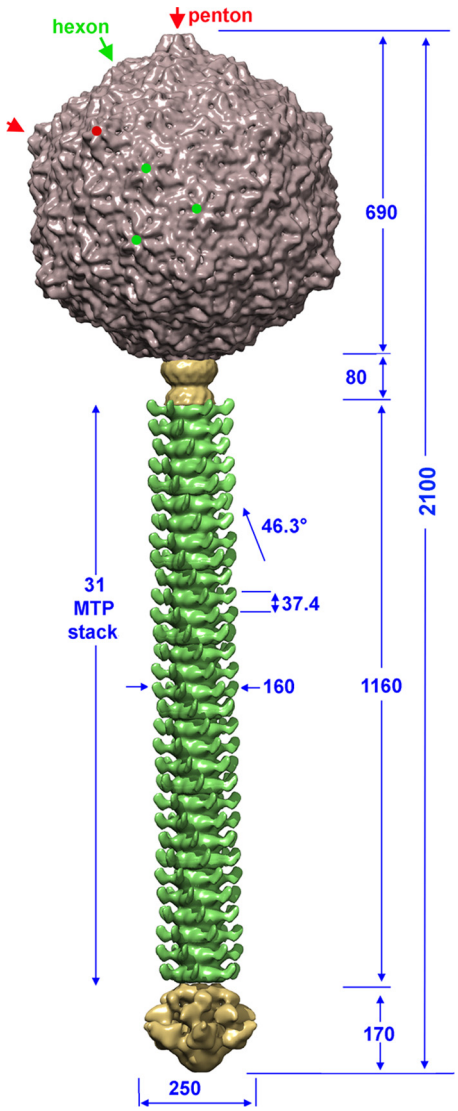

FIG 3 Overview of the full p2 phage assembled structure. This structure was generated by plugging the capsid (gray), connector (yellow), tail (green), and tail tip (dark yellow) into a low-resolution structure of phage p2. Dimensions are given in Å. Pentons are identified by red arrows and points, and hexons are identified by green arrows and points. The angle of rotation between MTP hexamers is 46.3°.

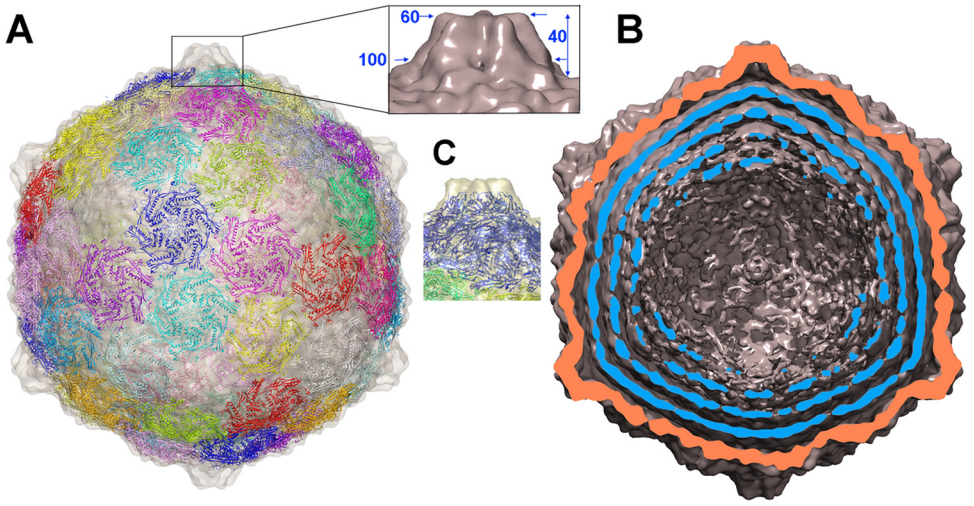

FIG 4 Cryo-EM reconstruction of the p2 mature capsid at a 13-Å resolution. (A) Transparent surface rendering of the icosahedral reconstruction low-pass filtered at 13 Å and viewed along an icosahedral 2-fold axis. The capsid measures 690 Å along its 5-fold axis. HK97 MCPs (66) have been fitted into the capsid's EM density map. (Inset) Close-up view of a protruding penton (distances in Å). (B) Cross section of the capsid reconstruction showing the external layer of the capsid (orange) and a few layers of the dsDNA genome organized as concentric shells (blue). (C) Close-up view of a capsid penton.

body (14). We have therefore subtracted from the phage EM structure the region of the reconstruction accounted for by the baseplate crystal structure, after removal of the nanobodies. The difference in density (Fig. 7A, yellow) corresponds well to the hexamer of ORF-15 that was missing from the crystal structure. The baseplate lower volume (Fig. 7, blue) was calculated at a 20-Å resolution from the crystal structure by Chimera. It was fitted into the corresponding EM density map, which was subsequently removed.

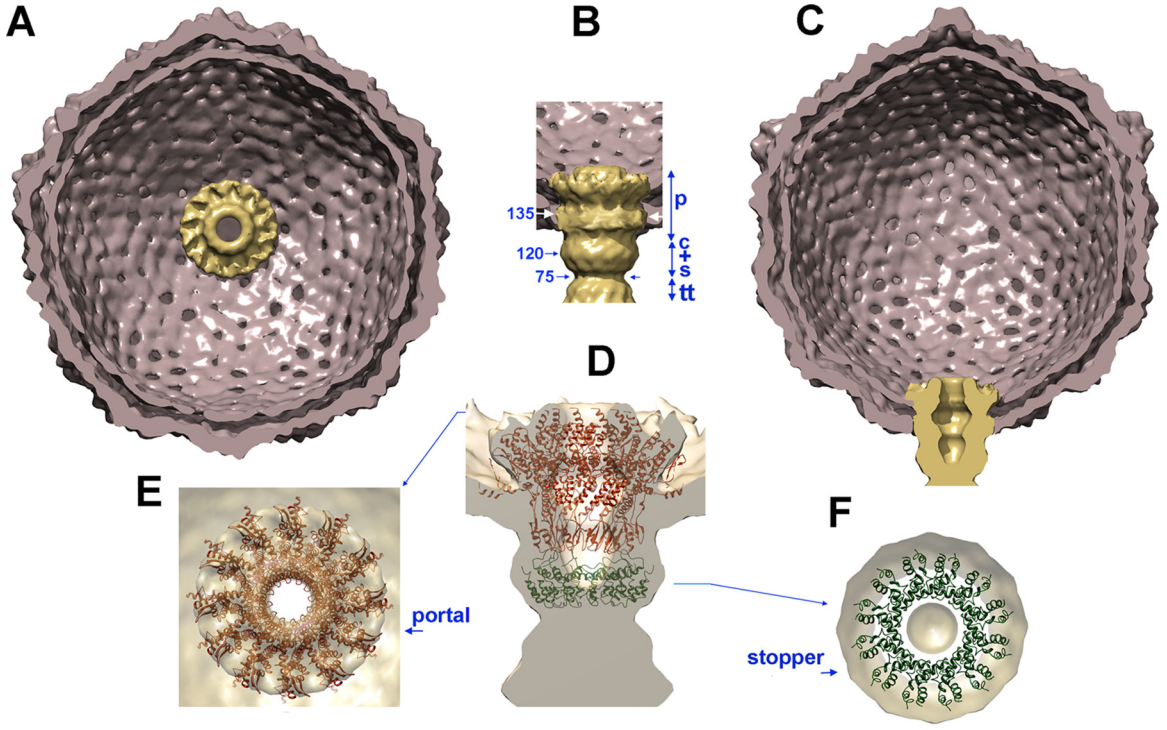

FIG 5 Reconstruction of the p2 connector at a unique capsid penton vertex at a 21-Å resolution. (A) Cross section of the p2 capsid (gray) showing the 12-fold portal (yellow) protruding inside it. (B) Side view of the p2 connector comprising the portal (p) (ORF-4) and the head completion proteins (c+s) (ORF-8 and ORF-9). The p2 tail terminator (TT) (ORF-10) belonging to the tail contacts the stopper at the constriction level. (C) Side-view (90° from panel A) cross section of the p2 capsid showing the connector tube, closed by the stopper (bottom). (D) Side view of the *Bacillus* phage SPP1 portal and the first head completion protein dodecamer (SPP1 gp15) fitted into the connector reconstruction. No space is left for the stopper (equivalent to SPP1 gp16) in this model. (E) Top view showing the fitting of the SPP1 portal dodecamer into the corresponding p2 EM density along the tail axis. (F) Top view showing the fitting of the SPP1 first head completion protein dodecamer (gp15) into the corresponding p2 EM density. Dimensions are given in Å.

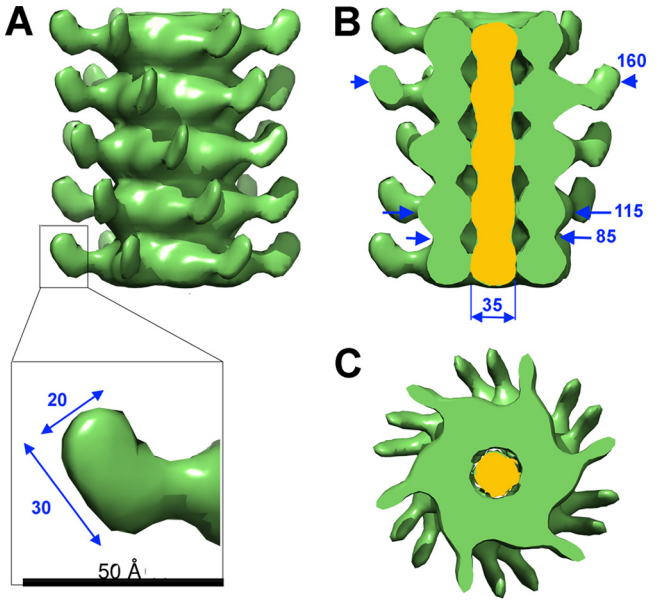

FIG 6 Reconstruction of the p2 tail at a 22-Å resolution. (A) Sixfold-averaged reconstruction of a p2 phage tail segment (5 MTP rings). (B) Cross section of the tail segment along its long axis revealing the internal TMP (orange). (C) Cross section of the tail segment orthogonal to its long axis (the coloring scheme is the same as in panel B). Dimensions are given in Å.

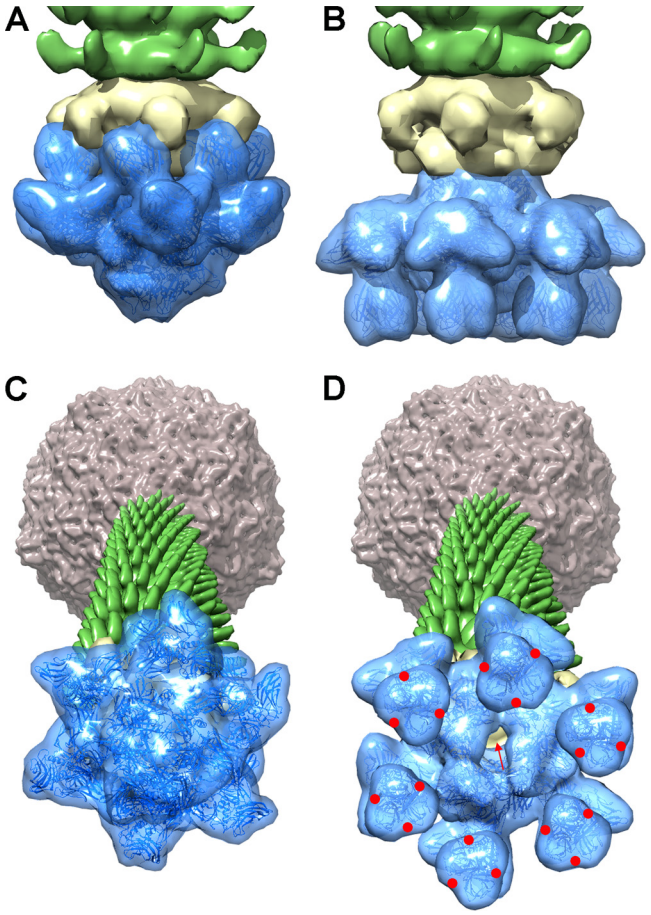

FIG 7 Composite X-ray–EM (22-Å) reconstruction of the p2 distal tail region (the baseplate). (A) A 20-Å electron density map (blue, ribbon structure inside) of the resting form (free virion) of the p2 baseplate crystal structure (14) was calculated and subtracted from the baseplate experimental EM map. The resulting difference map (yellow) corresponds to a Dit (ORF-15) hexamer. It is directly attached to a tail hexamer (green). (B) A 20-Å electron density map (blue, ribbon structure inside) of the activated form of the p2 baseplate crystal structure (14) was calculated and appended to the upper Dit EM map (yellow) attached to the tail's first MTP ring (green). (C and D) Perspective views of the reconstructions of the p2 phage in the resting (C) and activated (D) forms, showing in the forefront the baseplate structure, closed and opened, respectively. The red arrow identifies the open channel, and the red dots are located at the RBP saccharide binding sites in the activated p2 phage representation.

The same procedure was applied to the resting and activated forms of the baseplate (Fig. 7A and C, and B and D, respectively). These composite views illustrate that phage p2 contains two Dit hexamers organized back to back, in contrast to other Gram-positive-infecting phages characterized to date that harbor only one Dit hexamer (Fig. 7). The RBPs (ORF-18) are anchored via their N-terminal domain to the lower ORF-15 ring (as seen in the crystal structure) and via their C-terminal domain to the upper ORF-15 ring (as seen in the EM structure) (Fig. 7A). We present here models of the resting state (free p2 virion) as well as the Ca^{2+}-activated form of the p2 virion to illustrate the amplitude of the conformational changes involved in the activation process (Fig. 7). The RBPs undergo a 200° downward rotation to orient their 18 saccharide binding sites (six trimers) (Fig. 7D, red points) toward the host surface, concomitantly with the opening of the ORF-16 trimer (Tal), to form a central channel allowing ejection of the TMP from the tail tube, presumably across the cell wall, followed by genome release from the capsid, which will pass through the tail tube and enter the cytoplasm (Fig. 7D, red arrow).

RBP-pellicle interaction studies by surface plasmon resonance. As the RBPs of the baseplates have been proposed to bind to cell surface pellicles (6, 49), we used surface plasmon resonance (SPR) to check the specific interaction between the RBP and the host pellicle. Phages p2 and TP901-1 have different host specificities and recognize *L. lactis* MG1363 and *L. lactis* 3107, respectively. We therefore expected the affinity of the p2 RBP for the pellicle saccharide of *L. lactis* MG1363 to be higher than that of TP901-1. We biotinylated and attached the pellicle phosphopolysaccharide of *L. lactis* MG1363 to a C1 chip (GE Healthcare) coated with streptavidin. We then injected the trimeric RBP head (C-terminal) domain of phage p2 or the trimeric RBP of phage TP901-1 into the BIAcore-200 microfluidic instrument at increasing concentrations. For the p2 head domain, we obtained a saturating curve, which made it possible to calculate a K_d (dissociation constant) value of 230 ± 40 nM (Fig. 8A). For the TP901-1 RBP, we obtained a nonsaturating curve (Fig. 8B), confirming a higher affinity of p2 RBP for the phosphopolysaccharide of *L. lactis* MG1363. More significantly, when comparing the sensorgrams obtained with p2 and TP901-1 RBPs, the contact time of TP901-1 on the phosphopolysaccharide of *L. lactis* MG1363 was extremely short compared to that of p2. In practical terms, this means that phage TP901-1 would remain in contact with its nonspecific *L. lactis* host for a very short time.

DISCUSSION

We report here the complete EM structure of a lactococcal phage determined by single-particle analysis. Phage p2 is the flagship of the 936 group, which are the most prevalent lactococcal phages in industrial dairy fermentations worldwide. This phage is highly

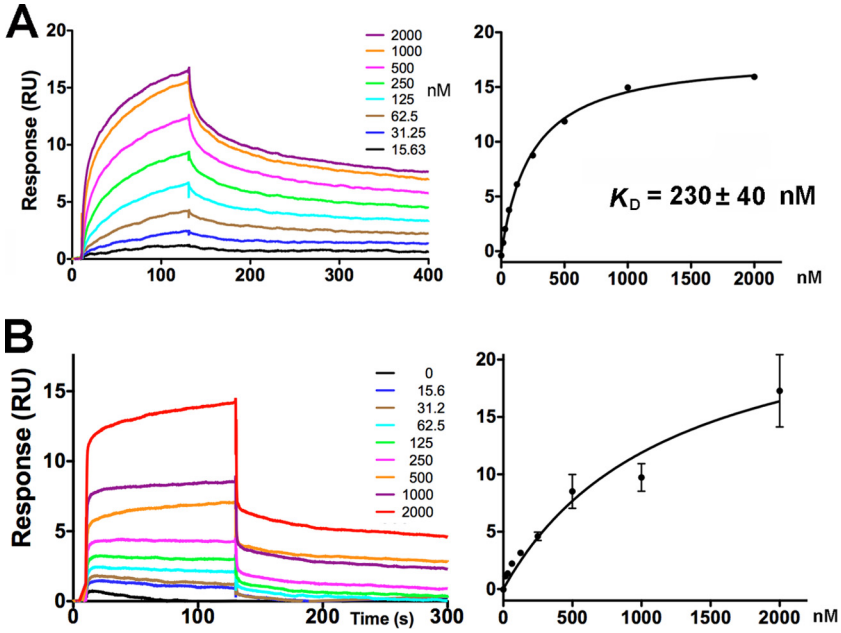

FIG 8 Phosphopolysaccharide binding to the p2 receptor binding protein. (A) SPR traces (left) and equilibrium curves (right) of the p2 RBP head domain injected over C1-grafted phosphopolysaccharide from *L. lactis* MG1363. (B) SPR traces and equilibrium curves of the TP901-1 RBP injected over C1-grafted phosphopolysaccharide from *L. lactis* MG1363.

virulent and requires Ca^{2+} to infect specific *L. lactis* cells, which is in contrast with the less prevalent lactococcal phages belonging to the P335 subgroup II (e.g., TP901-1 and Tuc2009) (15).

The shape of p2 icosahedral capsid is comparable to that of other siphophages. The capsid pentons are, however, more prominent than those of phage TP901-1 but akin to those of coliphage HK97. In contrast, the size of the p2 portal protein (ORF-4) is among the smallest, particularly in comparison to those of phage TP901-1 and *Bacillus* phage SPP1 (Table 3). The two putative head completion proteins of p2 (ORF-8 and ORF-9) are comparable to those of phage SPP1. The fit of the SPP1 portal and head completion protein 1 (gp15) into the p2 connector EM map was excellent (Fig. 4F and 5D). However, after fitting of these two proteins, no room was left in the p2 EM map to fit the stopper from SPP1 (gp16 [PDB accession number 2KCA]). Furthermore, in our docking, SPP1 gp15 is located at a position normally occupied by the stopper (ORF-9). We therefore propose that the short p2 portal protein (smaller by ~125 residues), compared to the SPP1 portal, leaves space that might be occupied by p2 ORF-8, similar in size to the SPP1 protein gp15. Space would still remain available for the stopper at the bottom of the EM density map (Fig. 5D to F), just above the tube constriction corresponding to the stopper/tail terminator junction (ORF-9/ORF-10).

One of the most striking features of the phage p2 structure is the presence of decorations covering the tail tube that are likely contributed by the MTP C-terminal domain. The p2 MTP (ORF-11; 301 amino acid residues) encompasses about twice as many residues as the TP901-1 MTP (169 residues) and is of a size comparable to that of the "long" MTP of *Bacillus* phage SPP1. In SPP1, the MTP-encoding gene (*orf17.1*) yields a majority of single-domain MTP (159 residues) contributing only to the formation of the tail tube. However, a ribosomal frameshift also leads to the production, but to a lesser extent, of a two-domain MTP (266 residues), which includes the tail-tube-decorating domain (50). The phage λ MTP (gpV) has 246 amino acid residues and is composed of an N-terminal conserved domain (gpV_N) (residues 1 to 159) forming the tail tube (51) and a C-terminal moiety (gpV_C) (residues 160 to 246) harboring an Ig-like fold probably involved in host cell wall saccharide interactions (52). Removal of the latter domain by genetic engineering resulted in a decrease of infectivity by a factor 100, illustrating its importance in the infection process (52). The mycobacteriophage Araucaria also exhibits tail decorations, and its MTP is 352 residues long (28). The ~190 extra MTP residues at the C terminus form its tail protrusions. HHpred data assigned the fold of an adhesin to this additional MTP domain of phage Araucaria. Interestingly, such Ig domains were also observed on phage capsids, such as that of the *Bacillus* podophage ϕ29 (53). The ~100 C-terminal residues of the ϕ29 MCP (gp8) exhibit a BIG2-type Ig fold, reported to mediate adhesion (12). We evaluated the length of the p2 MTP C-terminal domain to be at least ~120 residues, slightly larger than the Ig domain, because the MTP tube-forming domains are generally 160 to 180 residues long (Table 3). Taken together, these data point to a two-domain MTP (301 amino acids) in p2, with the N-terminal domain forming the tube (160 to 180 residues long) and the C-terminal domain (~120 residues) extending out of the tube. It is tempting to speculate that this C-terminal adhesin-like domain would be involved in some form of binding, possibly to the bacterial surface, a feature proposed previously for phages SPP1 and λ (50, 52).

The baseplate is a large macromolecular organelle involved in specific host recognition and attachment but presents different aspects depending on the phage. Phages that attach to host protein receptors display a long tail fiber (26). In Gram-negative bacteria such as *E. coli*, this is illustrated by phages T5 and lambda binding to porins (54, 55). In Gram-positive bacteria, this tail fiber is observed in *Bacillus* phage SPP1 (26, 56) and lactococcal phage c2

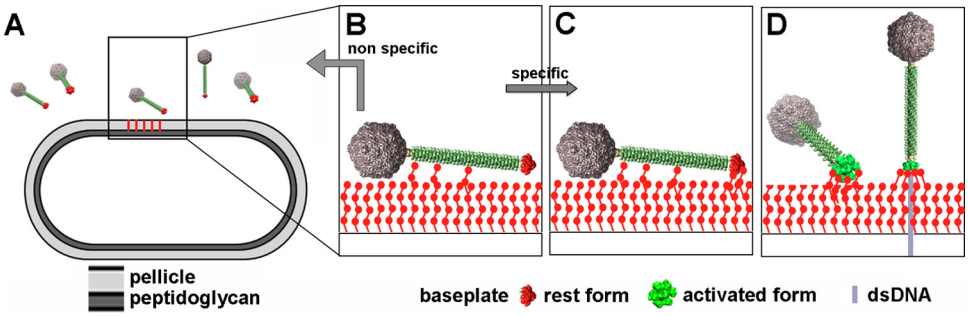

FIG 9 Proposed mechanism of infection of *L. lactis* MG1363 by phage p2. (A) Phages are in the vicinity of the host. (B) Weak interactions are established between the tail adhesins and, putatively, the pellicle. (C and D) Strain-specific lateral interactions may occur between the phage RBPs of the resting baseplate and the specific pellicle (C), leading, in the presence of Ca^{2+}, to baseplate activation, RBP rotation, and strong binding involving several of the 18 saccharide binding sites (D).

(57), both binding to a host membrane protein from the type 7 secretion system, YueB (56) and Pip (58), respectively. It has been proposed that lactococcal phages of the 936 and P335 groups may attach exclusively to polysaccharides (6, 49) and hence display a much larger macromolecular entity at their tail end, called the baseplate. The baseplate dimensions of lactococcal phage p2 and TP901-1 harbor a large number of RBPs, 18 and 54, respectively (14, 15). These baseplates have been found to be composed of a central axial core formed by the proteins Dit and Tal, also found in the tail tip phages (e.g., SPP1), and of a peripheral component formed by the RBPs, as in phage p2 (9, 14), as well as accessory proteins, as in phage TP901-1 (8, 15) or Tuc2009 (59, 60). The structure of the p2 baseplate was previously solved by X-ray crystallography, in both the nonactivated (closed) and activated (open, in the presence of Ca^{2+}) states. During activation, the six RBP trimers of p2 rotate by 200°, and the Tal trimer, located at the tail extremity, opens. In contrast, the crystal conformation of lactococcal phage TP901-1 is always in a conformation comparable to that of the activated p2 baseplate. The striking conformational differences observed between p2 (and the other 936 phages) and TP901-1 baseplates are correlated with functional consequences, since TP901-1 (and the P335 group) does not need Ca^{2+} for infection.

As indicated above, these large baseplates have been proposed to bind to cell surface polysaccharides (6, 49). *L. lactis* cells are covered by different structures of "pellicle" phosphopolysaccharides in a strain-specific way. These saccharides are synthesized by glycosyltransferases and other enzymes whose genes are located in close proximity in the *L. lactis* genome, the so-called pellicle gene cluster. It has been shown that in various *L. lactis* strains, these cassettes differ by the type and order of their gene components, which should have an impact on the pellicle polysaccharide motif and, consequently, phage sensitivity (61). Here, we show that p2 RBPs have a much higher affinity for and longer residence time in their specific *L. lactis* MG1363 pellicle than TP901-1 RBPs. Although the affinity is significant (~230 nM), it is much lower than affinities measured between protein-recognizing phages and their targets. For example, phage PRD1 binds to its host receptor through a unique interaction with a K_d of 0.2 nM (62). In the case of phages binding to saccharides, the weaker interaction at each site is compensated for by a high-avidity effect provided by the multiple receptor binding sites of their baseplates, 18 for p2 and 54 for TP901-1. It is most likely that the presence of a large baseplate at the distal end of the tail is the hallmark of phage adsorption to saccharide-based receptors.

Taken together, our results illustrate that phage p2 infection of *L. lactis* MG1363 is likely a multistep process (Fig. 9). First, the tail tube adhesion domains may interact with host cell wall saccharides in order to maintain the phage close to its target, as proposed for phage λ or SPP1 (Fig. 9B). Once near its host, the external accessible RBP sites of the baseplate in the nonactivated conformation may scan the hosts surface (Fig. 9C) in search of specific pellicle phosphohexasaccharide motifs, which differ between different *L. lactis* strains (61). If the number of specific binding events is large enough and Ca^{2+} is available, the mechanical pull induced by this binding may destabilize the rest conformation of the baseplate and disrupt the interaction between the second Dit "arm" (14) and the RBP head domain. The RBPs would then initiate a 200° rotation toward the host's surface, a movement coupled with Tal opening (14) (Fig. 9D). This large conformational change is probably somehow coupled to a signal to the stopper to open (26), releasing the dsDNA from the phage capsid. The dsDNA would in turn push out the TMP, which is suspected to guide delivery to the cytoplasm (54, 63, 64). In a majority of phages, the Tal protein harbors at its C terminus endolysin activity to digest the peptidoglycan and form a hole permitting the passage of the MTP and dsDNA at the onset of infection. However, no peptidase sequence could be identified in the phage p2 genome as for the other phages of the 936 group (20). These phages infect their host only during the exponential phase, while those from the P335 subgroup II, having a peptidase, also infect the host in stationary phase (20, 65). The peptidoglycan is cross-linked during the stationary phase, and these P335 phages probably need the peptidase activity for their DNA to penetrate the cell wall.

It is most likely that the two types of baseplates and adhesion mechanisms (p2 versus TP901-1) are widespread in the *Siphoviridae* family. Examination of several electron micrographs of siphophages from various bacterial species (http://www.phage.ulaval.ca/) reveals the presence a large number of them with baseplates resembling that of p2 or TP901-1. In this context, the activation mechanism of phage p2 might be relevant to a large range of phages.

ACKNOWLEDGMENTS

This work was supported in part by grants from the Marseille-Nice Génopole, the CNRS, and the Agence Nationale de la Recherche (grants ANR-07-BLAN-0095, Siphophages, and ANR-11-BSV8-004-01, Lactophages). M.H. acknowledges financial support from the European Union/NOE (NOE grant PE0748), from the Dutch Ministry of Economic Affairs (Cyttron project BIBCR_PX0948), and from the BBSRC (grant

BB/G015236/1). This work was also supported in part by the NSERC of Canada (Strategic Program) as well as by the MDEIE (PSR:PSIIRI program). S.M. holds a Tier 1 Canada Research Chair in bacteriophages.

REFERENCES

1. **Ackermann HW.** 2012. Bacteriophage electron microscopy. Adv. Virus Res. **82:**1–32.
2. **Deveau H, Labrie SJ, Chopin MC, Moineau S.** 2006. Biodiversity and classification of lactococcal phages. Appl. Environ. Microbiol. **72:**4338–4346.
3. **Samson JE, Moineau S.** 2013. Bacteriophages in food fermentations: new frontiers in a continuous arms race. Annu. Rev. Food Sci. Technol. **4:**347–368.
4. **Mooney DT, Jann M, Geller BL.** 2006. Subcellular location of phage infection protein (Pip) in Lactococcus lactis. Can. J. Microbiol. **52:**664–672.
5. **Valyasevi R, Sandine WE, Geller BL.** 1991. A membrane protein is required for bacteriophage c2 infection of Lactococcus lactis subsp. lactis C2. J. Bacteriol. **173:**6095–6100.
6. **Chapot-Chartier MP, Vinogradov E, Sadovskaya I, Andre G, Mistou MY, Trieu-Cuot P, Furlan S, Bidnenko E, Courtin P, Pechoux C, Hols P, Dufrene YF, Kulakauskas S.** 2010. Cell surface of Lactococcus lactis is covered by a protective polysaccharide pellicle. J. Biol. Chem. **285:**10464–10471.
7. **Ricagno S, Campanacci V, Blangy S, Spinelli S, Tremblay D, Moineau S, Tegoni M, Cambillau C.** 2006. Crystal structure of the receptor-binding protein head domain from Lactococcus lactis phage bIL170. J. Virol. **80:**9331–9335.
8. **Spinelli S, Campanacci V, Blangy S, Moineau S, Tegoni M, Cambillau C.** 2006. Modular structure of the receptor binding proteins of Lactococcus lactis phages. The RBP structure of the temperate phage TP901-1. J. Biol. Chem. **281:**14256–14262.
9. **Spinelli S, Desmyter A, Verrips CT, de Haard HJ, Moineau S, Cambillau C.** 2006. Lactococcal bacteriophage p2 receptor-binding protein structure suggests a common ancestor gene with bacterial and mammalian viruses. Nat. Struct. Mol. Biol. **13:**85–89.
10. **Tremblay DM, Tegoni M, Spinelli S, Campanacci V, Blangy S, Huyghe C, Desmyter A, Labrie S, Moineau S, Cambillau C.** 2006. Receptor-binding protein of Lactococcus lactis phages: identification and characterization of the saccharide receptor-binding site. J. Bacteriol. **188:**2400–2410.
11. **Veesler D, Dreier B, Blangy S, Lichiere J, Tremblay D, Moineau S, Spinelli S, Tegoni M, Pluckthun A, Campanacci V, Cambillau C.** 2009. Crystal structure and function of a DARPin neutralizing inhibitor of lactococcal phage TP901-1: comparison of DARPin and camelid VHH binding mode. J. Biol. Chem. **284:**30718–30726.
12. **Siponen M, Spinelli S, Blangy S, Moineau S, Cambillau C, Campanacci V.** 2009. Crystal structure of a chimeric receptor binding protein constructed from two lactococcal phages. J. Bacteriol. **191:**3220–3225.
13. **Bebeacua C, Bron P, Lai L, Vegge CS, Brondsted L, Spinelli S, Campanacci V, Veesler D, van Heel M, Cambillau C.** 2010. Structure and molecular assignment of lactococcal phage TP901-1 baseplate. J. Biol. Chem. **285:**39079–39086.
14. **Sciara G, Bebeacua C, Bron P, Tremblay D, Ortiz-Lombardia M, Lichiere J, van Heel M, Campanacci V, Moineau S, Cambillau C.** 2010. Structure of lactococcal phage p2 baseplate and its mechanism of activation. Proc. Natl. Acad. Sci. U. S. A. **107:**6852–6857.
15. **Veesler D, Spinelli S, Mahony J, Lichiere J, Blangy S, Bricogne G, Legrand P, Ortiz-Lombardia M, Campanacci V, van Sinderen D, Cambillau C.** 2012. Structure of the phage TP901-1 1.8 MDa baseplate suggests an alternative host adhesion mechanism. Proc. Natl. Acad. Sci. U. S. A. **109:**8954–8958.
16. **Bebeacua C, Lai L, Vegge CS, Brondsted L, van Heel M, Veesler D, Cambillau C.** 2013. Visualizing a complete Siphoviridae member by single-particle electron microscopy: the structure of lactococcal phage TP901-1. J. Virol. **87:**1061–1068.
17. **De Haard HJ, Bezemer S, Ledeboer AM, Muller WH, Boender PJ, Moineau S, Coppelmans MC, Verkleij AJ, Frenken LG, Verrips CT.** 2005. Llama antibodies against a lactococcal protein located at the tip of the phage tail prevent phage infection. J. Bacteriol. **187:**4531–4541.
18. **Desmyter A, Farenc C, Mahony J, Spinelli S, Bebeacua C, Blangy S, Veesler D, van Sinderen D, Cambillau C.** 2013. Viral infection modulation and neutralization by camelid nanobodies. Proc. Natl. Acad. Sci. U. S. A. **110:**E1371–E1379. doi:10.1073/pnas.1301336110.
19. **Hultberg A, Tremblay DM, de Haard H, Verrips T, Moineau S, Hammarstrom L, Marcotte H.** 2007. Lactobacilli expressing llama VHH fragments neutralise Lactococcus phages. BMC Biotechnol. **7:**58. doi:10.1186/1472-6750-7-58.
20. **Mahony J, Martel B, Tremblay DM, Neve H, Heller KJ, Moineau S, van Sinderen D.** 2013. Identification of a new P335 subgroup through molecular analysis of lactococcal phages Q33 and BM13. Appl. Environ. Microbiol. **79:**4401–4409.
21. **Hu B, Margolin W, Molineux IJ, Liu J.** 2013. The bacteriophage t7 virion undergoes extensive structural remodeling during infection. Science **339:**576–579.
22. **Lander GC, Tang L, Casjens SR, Gilcrease EB, Prevelige P, Poliakov A, Potter CS, Carragher B, Johnson JE.** 2006. The structure of an infectious P22 virion shows the signal for headful DNA packaging. Science **312:**1791–1795.
23. **Simpson AA, Tao Y, Leiman PG, Badasso MO, He Y, Jardine PJ, Olson NH, Morais MC, Grimes S, Anderson DL, Baker TS, Rossmann MG.** 2000. Structure of the bacteriophage phi29 DNA packaging motor. Nature **408:**745–750.
24. **Effantin G, Boulanger P, Neumann E, Letellier L, Conway JF.** 2006. Bacteriophage T5 structure reveals similarities with HK97 and T4 suggesting evolutionary relationships. J. Mol. Biol. **361:**993–1002.
25. **Lhuillier S, Gallopin M, Gilquin B, Brasiles S, Lancelot N, Letellier G, Gilles M, Dethan G, Orlova EV, Couprie J, Tavares P, Zinn-Justin S.** 2009. Structure of bacteriophage SPP1 head-to-tail connection reveals mechanism for viral DNA gating. Proc. Natl. Acad. Sci. U. S. A. **106:**8507–8512.
26. **Plisson C, White HE, Auzat I, Zafarani A, Sao-Jose C, Lhuillier S, Tavares P, Orlova EV.** 2007. Structure of bacteriophage SPP1 tail reveals trigger for DNA ejection. EMBO J. **26:**3720–3728.
27. **White HE, Sherman MB, Brasiles S, Jacquet E, Seavers P, Tavares P, Orlova EV.** 2012. Capsid structure and its stability at the late stages of bacteriophage SPP1 assembly. J. Virol. **86:**6768–6777.
28. **Sassi M, Bebeacua C, Drancourt M, Cambillau C.** 2013. The first structure of a mycobacteriophage, the Mycobacterium abscessus subsp. bolletii phage Araucaria. J. Virol. **87:**8099–8109.
29. **Chibani Azaiez SR, Fliss I, Simard RE, Moineau S.** 1998. Monoclonal antibodies raised against native major capsid proteins of lactococcal c2-like bacteriophages. Appl. Environ. Microbiol. **64:**4255–4259.
30. **Sambrook J, Russell DW.** 2001. Molecular cloning: a laboratory manual, 3rd ed. Cold Spring Harbor Laboratory Press, Cold Spring Harbor, NY.
31. **van Heel M, Harauz G, Orlova EV, Schmidt R, Schatz M.** 1996. A new generation of the IMAGIC image processing system. J. Struct. Biol. **116:**17–24.
32. **van Heel M, Schatz M.** 2005. Fourier shell correlation threshold criteria. J. Struct. Biol. **151:**250–262.
33. **Egelman EH.** 2007. The iterative helical real space reconstruction method: surmounting the problems posed by real polymers. J. Struct. Biol. **157:**83–94.
34. **Owen CH, Morgan DG, DeRosier DJ.** 1996. Image analysis of helical objects: the Brandeis Helical Package. J. Struct. Biol. **116:**167–175.
35. **Grun CH, van Vliet SJ, Schiphorst WE, Bank CM, Meyer S, van Die I, van Kooyk Y.** 2006. One-step biotinylation procedure for carbohydrates to study carbohydrate-protein interactions. Anal. Biochem. **354:**54–63.
36. **Myszka DG.** 2000. Kinetic, equilibrium, and thermodynamic analysis of macromolecular interactions with BIACORE. Methods Enzymol. **323:**325–340.
37. **Siponen M, Sciara G, Villion M, Spinelli S, Lichiere J, Cambillau C, Moineau S, Campanacci V.** 2009. Crystal structure of ORF12 from Lactococcus lactis phage p2 identifies a tape measure protein chaperone. J. Bacteriol. **191:**728–734.
38. **Brondsted L, Ostergaard S, Pedersen M, Hammer K, Vogensen FK.** 2001. Analysis of the complete DNA sequence of the temperate bacteriophage TP901-1: evolution, structure, and genome organization of lactococcal bacteriophages. Virology **283:**93–109.
39. **Chai S, Szepan U, Luder G, Trautner TA, Alonso JC.** 1993. Sequence analysis of the left end of the Bacillus subtilis bacteriophage SPP1 genome. Gene **129:**41–49.
40. **Labrie SJ, Tremblay DM, Moisan M, Villion M, Magadan AH, Campanacci V, Cambillau C, Moineau S.** 2012. Involvement of the major capsid protein and two early-expressed phage genes in the activity of the

lactococcal abortive infection mechanism AbiT. Appl. Environ. Microbiol. **78:**6890–6899.
41. **Veesler D, Quispe J, Grigorieff N, Potter CS, Carragher B, Johnson JE.** 2012. Maturation in action: cryoEM study of a viral capsid caught during expansion. Structure **20:**1384–1390.
42. **Smith DE, Tans SJ, Smith SB, Grimes S, Anderson DL, Bustamante C.** 2001. The bacteriophage straight phi29 portal motor can package DNA against a large internal force. Nature **413:**748–752.
43. **Veesler D, Cambillau C.** 2011. A common evolutionary origin for tailed-bacteriophage functional modules and bacterial machineries. Microbiol. Mol. Biol. Rev. **75:**423–433.
44. **Wikoff WR, Liljas L, Duda RL, Tsuruta H, Hendrix RW, Johnson JE.** 2000. Topologically linked protein rings in the bacteriophage HK97 capsid. Science **289:**2129–2133.
45. **Lebedev AA, Krause MH, Isidro AL, Vagin AA, Orlova EV, Turner J, Dodson EJ, Tavares P, Antson AA.** 2007. Structural framework for DNA translocation via the viral portal protein. EMBO J. **26:**1984–1994.
46. **Goulet A, Lai-Kee-Him J, Veesler D, Auzat I, Robin G, Shepherd DA, Ashcroft AE, Richard E, Lichiere J, Tavares P, Cambillau C, Bron P.** 2011. The opening of the SPP1 bacteriophage tail, a prevalent mechanism in Gram-positive-infecting siphophages. J. Biol. Chem. **286:**25397–25405.
47. **Veesler D, Robin G, Lichiere J, Auzat I, Tavares P, Bron P, Campanacci V, Cambillau C.** 2010. Crystal structure of bacteriophage SPP1 distal tail protein (gp19.1): a baseplate hub paradigm in Gram-positive infecting phages. J. Biol. Chem. **285:**36666–36673.
48. **Pedersen M, Ostergaard S, Bresciani J, Vogensen FK.** 2000. Mutational analysis of two structural genes of the temperate lactococcal bacteriophage TP901-1 involved in tail length determination and baseplate assembly. Virology **276:**315–328.
49. **Andre G, Kulakauskas S, Chapot-Chartier MP, Navet B, Deghorain M, Bernard E, Hols P, Dufrene YF.** 2010. Imaging the nanoscale organization of peptidoglycan in living Lactococcus lactis cells. Nat. Commun. **1:**1. doi:10.1038/ncomms1011.
50. **Auzat I, Droge A, Weise F, Lurz R, Tavares P.** 2008. Origin and function of the two major tail proteins of bacteriophage SPP1. Mol. Microbiol. **70:**557–569.
51. **Pell LG, Kanelis V, Donaldson LW, Howell PL, Davidson AR.** 2009. The phage lambda major tail protein structure reveals a common evolution for long-tailed phages and the type VI bacterial secretion system. Proc. Natl. Acad. Sci. U. S. A. **106:**4160–4165.
52. **Pell LG, Gasmi-Seabrook GM, Morais M, Neudecker P, Kanelis V, Bona D, Donaldson LW, Edwards AM, Howell PL, Davidson AR, Maxwell KL.** 2010. The solution structure of the C-terminal Ig-like domain of the bacteriophage lambda tail tube protein. J. Mol. Biol. **403:**468–479.
53. **Morais MC, Choi KH, Koti JS, Chipman PR, Anderson DL, Rossmann MG.** 2005. Conservation of the capsid structure in tailed dsDNA bacteriophages: the pseudoatomic structure of phi29. Mol. Cell **18:**149–159.
54. **Boulanger P, Jacquot P, Plancon L, Chami M, Engel A, Parquet C, Herbeuval C, Letellier L.** 2008. Phage T5 straight tail fiber is a multifunctional protein acting as a tape measure and carrying fusogenic and muralytic activities. J. Biol. Chem. **283:**13556–13564.
55. **Flayhan A, Wien F, Paternostre M, Boulanger P, Breyton C.** 2012. New insights into pb5, the receptor binding protein of bacteriophage T5, and its interaction with its Escherichia coli receptor FhuA. Biochimie **94:**1982–1989.
56. **Sao-Jose C, Lhuillier S, Lurz R, Melki R, Lepault J, Santos MA, Tavares P.** 2006. The ectodomain of the viral receptor YueB forms a fiber that triggers ejection of bacteriophage SPP1 DNA. J. Biol. Chem. **281:**11464–11470.
57. **Lubbers MW, Waterfield NR, Beresford TP, Le Page RW, Jarvis AW.** 1995. Sequencing and analysis of the prolate-headed lactococcal bacteriophage c2 genome and identification of the structural genes. Appl. Environ. Microbiol. **61:**4348–4356.
58. **Babu KS, Spence WS, Monteville MR, Geller BL.** 1995. Characterization of a cloned gene (pip) from Lactococcus lactis required for phage infection. Dev. Biol. Stand. **85:**569–575.
59. **Mc Grath S, Neve H, Seegers JF, Eijlander R, Vegge CS, Brondsted L, Heller KJ, Fitzgerald GF, Vogensen FK, van Sinderen D.** 2006. Anatomy of a lactococcal phage tail. J. Bacteriol. **188:**3972–3982.
60. **Sciara G, Blangy S, Siponen M, Mc Grath S, van Sinderen D, Tegoni M, Cambillau C, Campanacci V.** 2008. A topological model of the baseplate of lactococcal phage Tuc2009. J. Biol. Chem. **283:**2716–2723.
61. **Mahony J, Kot W, Murphy J, Ainsworth S, Neve H, Hansen LH, Heller KJ, Sorensen SJ, Hammer K, Cambillau C, Vogensen FK, van Sinderen D.** 2013. Investigation of the relationship between lactococcal host cell wall polysaccharide genotype and 936 phage receptor binding protein phylogeny. Appl. Environ. Microbiol. **79:**4385–4392.
62. **Grahn AM, Caldentey J, Bamford JK, Bamford DH.** 1999. Stable packaging of phage PRD1 DNA requires adsorption protein P2, which binds to the IncP plasmid-encoded conjugative transfer complex. J. Bacteriol. **181:**6689–6696.
63. **Bebeacua C, Lorenzo Fajardo JC, Blangy S, Spinelli S, Bollmann S, Neve H, Cambillau C, Heller KJ.** 2013. X-ray structure of a superinfection exclusion lipoprotein from phage TP-J34 and identification of the tape measure protein as its target. Mol. Microbiol. **89:**152–165.
64. **Collins B, Bebeacua C, Mahony J, Blangy S, Douillard FP, Veesler D, Cambillau C, van Sinderen D.** 2013. Structure and functional analysis of the host recognition device of lactococcal phage tuc2009. J. Virol. **87:**8429–8440.
65. **Stockdale SR, Mahony J, Courtin P, Chapot-Chartier MP, van Pijkeren JP, Britton RA, Neve H, Heller KJ, Aideh B, Vogensen FK, van Sinderen D.** 2013. The lactococcal phages Tuc2009 and TP901-1 incorporate two alternate forms of their tail fiber into their virions for infection specialization. J. Biol. Chem. **288:**5581–5590.
66. **Helgstrand C, Wikoff WR, Duda RL, Hendrix RW, Johnson JE, Liljas L.** 2003. The refined structure of a protein catenane: the HK97 bacteriophage capsid at 3.44 A resolution. J. Mol. Biol. **334:**885–899.